

Observation of a warped helical spin-texture in Bi_2Se_3 from circular dichroism angle-resolved photoemission spectroscopy

Y. H. Wang^{1,2}, D. Hsieh¹, D. Pilon¹, L. Fu², D. R. Gardner¹, Y. S. Lee¹, and N. Gedik¹

¹*Department of Physics, Massachusetts Institute of Technology, Cambridge MA 02139, USA and*

²*Department of Physics, Harvard University, Cambridge MA 02138, USA*

A differential coupling of topological surface states to left- versus right-circularly polarized light is the basis of many opto-spintronics applications of topological insulators. Here we report direct evidence of circular dichroism from the surface states of Bi_2Se_3 using a laser-based time-of-flight angle-resolved photoemission spectroscopy. By employing a novel sample rotational analysis, we resolve unusual modulations in the circular dichroism photoemission pattern as a function of both energy and momentum, which perfectly mimic the predicted but hitherto un-observed three-dimensional warped spin-texture of the surface states. By developing a microscopic theory of photoemission from topological surface states, we show that this correlation is a natural consequence of spin-orbit coupling. These results suggest that our technique may be a powerful probe of the spin-texture of spin-orbit coupled materials in general.

Three-dimensional topological insulators [1–3] are an intensely researched phase of matter owing to their unique spin-helical metallic surfaces, where the spin direction is locked to the wavevector and winds by 2π around the Fermi surface [4–6]. Spin-dependent absorption of circularly polarized light has recently been predicted to generate highly spin-polarized surface electrical currents whose direction can be switched by the light helicity [7–9]. However, a demonstration of spin-dependent differential absorption of left- versus right-circularly polarized light [circular dichroism (CD)] from the surface states (SS) has evaded conventional probes such as transport and optics because of the combined need for energy-momentum resolution and surface sensitivity.

In this Letter, we map the variation of the CD in the photoemission intensity [10–15] over the full surface band structure of the topological insulator Bi_2Se_3 [16, 17] using a laser-based time-of-flight angle-resolved photoemission spectroscopy (TOF-ARPES) technique. Our results show a strong CD from the SS in agreement with a recent work on $\text{Cu}_x\text{Bi}_2\text{Se}_3$ [18]. However, owing to our ultra-high polarization purity and our novel sample rotational analysis, we uniquely resolve fine modulations in the CD pattern as a function of energy and momentum that perfectly follow the predicted [19, 20], but so far un-detected [6], three-dimensional spin-texture of Bi_2Se_3 . By developing a microscopic theory of photoemission from topological SS, we show that such modulations naturally arise from the coupling of the circularly polarized light to the surface spin-texture via spin-orbit interactions. Excellent agreement between our results and theory suggests that our technique is an efficient and sensitive measure of all three components of the surface spin-texture.

The experimental setup is shown in Fig. 1(a). Single crystals of Bi_2Se_3 are cleaved along their (111) surface at room temperature under ultra-high-vacuum ($< 6 \times 10^{-11}$ Torr). Femtosecond laser pulses from a Ti:Sapph amplifier are frequency quadrupled to 6.2eV and then circularly polarized to $> 99\%$ purity with a quarter wave-

plate. Strain induced birefringence from the vacuum windows and dichroism from all optical elements following the quarter wave-plate, which can ruin the purity of circular polarization, were carefully compensated in our experiment [21]. Conventional hemispherical ARPES analyzers rely on the deflection of electron paths along one spatial dimension to measure electronic dispersion along one direction in momentum space. In contrast, our TOF-ARPES analyzer is developed for pulsed photon sources and resolves electron energies through their flight time from sample to detector, which enables measuring dispersion spectra $I(E, k_x, k_y)$ simultaneously over two dimensional momentum space. Complete spectra of Bi_2Se_3 (surface Dirac cone plus bulk conduction band) obtained with TOF-ARPES is shown in Fig.1(b). This ability to measure the entire bandstructure simultaneously eliminates experimental geometry induced matrix element effects [22] that may obscure the intrinsic CD pattern and allows for direct comparison of CD-ARPES intensities across different phase space points.

To investigate whether CD is exhibited by Bi_2Se_3 and if it has bulk and/or surface state origin, we measure spectra like in Fig.1(b) using left- and right-circularly polarized light and then take their difference to obtain the CD spectrum $\Delta I(E, k_x, k_y)$. As shown in Figs. 1(c)-(d), there is clear CD from the surface Dirac cone of Bi_2Se_3 and not from the bulk conduction band. The CD pattern exhibits perfectly odd reflection symmetry about the photon scattering plane when it is parallel to the $\bar{\Gamma}\bar{M}$ direction [Fig. 1(e)], which is expected from crystal mirror symmetry. However this odd reflection symmetry is lifted when the scattering plane is along a non mirror-symmetric direction such as $\bar{\Gamma}\bar{K}$ [Fig. 1(f)], which is evidence that the CD pattern is intrinsic to the sample.

Having shown that CD is intrinsic to the sample and present for the SS, we first focus on its fine features in the low energy region [$\pm 0.1\text{eV}$ relative to the Dirac point (DP)] where the Fermi surface is circular. Fig. 1(d)

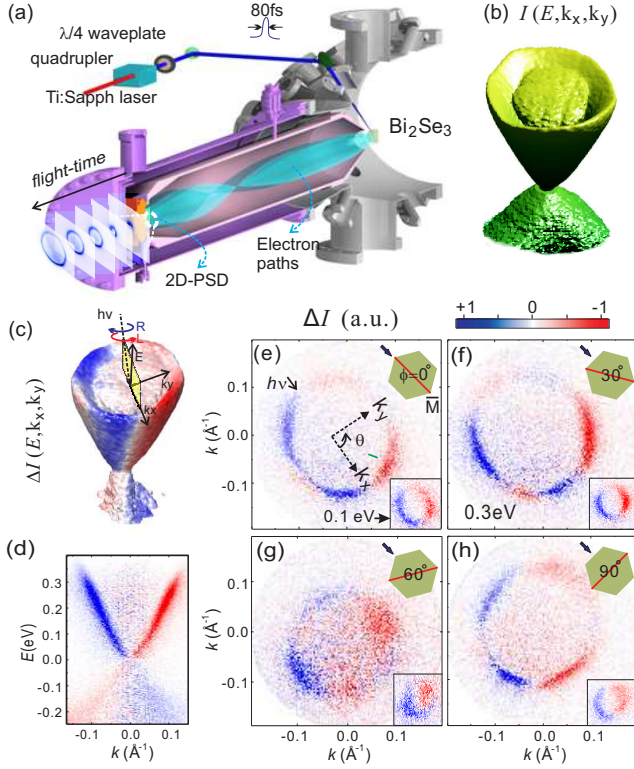


FIG. 1. (a) Schematic of a time-of-flight based angle-resolved photoemission spectrometer. PSD: position-sensitive detector. (b) A typical iso-intensity surface in (E, k_x, k_y) space from Bi_2Se_3 collected simultaneously using linearly polarized photons. (c) Difference of TOF-ARPES data measured using right- and left-circularly polarized light. $h\nu$ denotes the incident photon direction. (d) $E - k$ cut through the CD data volume in (c) along the angle denoted by the green dash in (e). (e-h) Constant energy slices through (c) at the Fermi level and at 0.1eV above the DP (insets) for sample rotation angles of $\phi = 0^\circ, 30^\circ, 60^\circ$ and 90° respectively. Green hexagons represent the Brillouin zone of $\text{Bi}_2\text{Se}_3(111)$, red lines are the mirror planes and the arrow denotes the photon incident direction.

shows that at a constant energy the sign of CD is reversed for states of opposite momentum and is reversed again across the DP. Furthermore, the CD pattern is invariant under rotation (ϕ) of the crystal mirror plane relative to the scattering plane [Figs. 1(e)-(h) insets]. These behaviors match the known in-plane spin texture in the low energy region, which are tangential to the rotationally isotropic constant energy contours [4, 5] and reverse chirality across the DP.

The CD patterns change drastically away from the low energy region ($|E| > 0.1\text{eV}$), where the Fermi surface evolves from being circular to hexagonal in shape [19, 23]. Here we observe new modulations in the magnitude and sign of CD as a function of the angle θ around the constant energy contours [Figs. 1(e)-(h)]. In particular, extrema along the k_y axis (at $\theta = 90^\circ$ and 270°) at low energy [Figs. 1(e)-(h) insets] become nodes in the

high energy $\phi = 0^\circ$ spectrum [Fig. 1(e)]. Furthermore, in stark contrast to the low energy region, CD patterns at high energy undergo dramatic changes as ϕ is varied. For instance, the nodes along k_y in the Fig. 1(e) spectrum become extrema again in the $\phi = 60^\circ$ spectrum [Fig. 1(g)] and only repeats itself under $\phi = 120^\circ$ rotations, consistent with the symmetry of the underlying lattice. This is reminiscent of the predicted θ dependence of the out-of-plane component of spin $\langle S_z \rangle$ at high energies [19, 20], which goes from minimum to maximum under $\phi = 60^\circ$ rotation. Such behavior has been observed using Mott polarimetry only in Bi_2Te_3 [5] but not in Bi_2Se_3 [6] owing to the much larger value of $\langle S_z \rangle$ in the former. Given that the overall CD patterns observed closely follow the predicted spin-texture of the SS, we investigate their possible connection by developing a standard model of photoemission from topological SS.

The microscopic Hamiltonian for a system with spin-orbit coupling is given by:

$$H = \frac{\vec{P}^2}{2m} + V(\vec{r}) + \frac{\hbar}{4m^2c^2} (\vec{P} \times \vec{\nabla} V) \cdot \vec{s} \quad (1)$$

where \vec{P} is momentum operator, $V(\vec{r})$ is the crystal potential, and \vec{s} is the electron spin. Coupling to an electromagnetic field is obtained via $\vec{P} \rightarrow \vec{P} - e\vec{A}$, where \vec{A} is the photon vector potential, such that to first order in \vec{A} :

$$H(\vec{A}) = H - \vec{P} \cdot \vec{A} \quad (2)$$

where $\vec{P} \equiv \frac{e}{m}\vec{P} - \frac{\hbar e}{4m^2c^2}(\vec{\nabla} V \times \vec{s})$. The photoemission matrix element between the initial and final states is given by

$$M(\vec{k}, f) = \langle f_{\vec{k}} | \vec{P} \cdot \vec{A} | \vec{k} \rangle \quad (3)$$

where $\vec{A} \equiv \int dt \vec{A}(t) e^{i\omega t}$ is the Fourier transform of \vec{A} and $|f_{\vec{k}}\rangle$ is the bulk final state. The initial state $|\vec{k}\rangle = u_{\vec{k}}|\phi_+^i\rangle + v_{\vec{k}}|\phi_-^i\rangle$ is a linear combination of two-fold degenerate pseudospin states $|\phi_{\pm}^i\rangle$ at the DP that are eigenstates of total angular momentum (orbital plus spin), which is widely used in standard $k \cdot p$ descriptions of topological SS [2, 17, 19, 24]. Because of strong spin-orbit coupling, only pseudospin is a good quantum number [19]. The coefficients $u_{\vec{k}}$ and $v_{\vec{k}}$ determine the expectation value of three pseudospin components: $\langle S_x \rangle_{\vec{k}} = \hbar(u_{\vec{k}}^* v_{\vec{k}} + v_{\vec{k}}^* u_{\vec{k}})$, $\langle S_y \rangle_{\vec{k}} = \hbar(v_{\vec{k}}^* u_{\vec{k}} - i u_{\vec{k}}^* v_{\vec{k}})$, $\langle S_z \rangle_{\vec{k}} = \hbar(|u_{\vec{k}}|^2 - |v_{\vec{k}}|^2)$. Importantly, because spin is directly proportional to pseudospin [19], we refer to the two interchangeably. For circularly polarized light incident onto the surface with wavevector in the xz plane, $\vec{A}(t) = (A_x \sin \omega t, A_y \cos \omega t, A_z \sin \omega t)$ and $\vec{A} = (-iA_x, A_y, -iA_z)$. Straight-forward application of time-reversal and crystal symmetries [21] yield the following expression for the photoemission transition rate:

$$I(\vec{k}) = a^2 (|\mathcal{A}_x|^2 + |\mathcal{A}_y|^2) + b^2 |\mathcal{A}_z|^2 + a^2 \text{Im}(\mathcal{A}_x \mathcal{A}_y^*) \langle S_z \rangle_{\vec{k}} + 2ab \text{Im}[\mathcal{A}_x^* \mathcal{A}_z \langle S_y \rangle_{\vec{k}} - \mathcal{A}_y^* \mathcal{A}_z \langle S_x \rangle_{\vec{k}}] \quad (4)$$

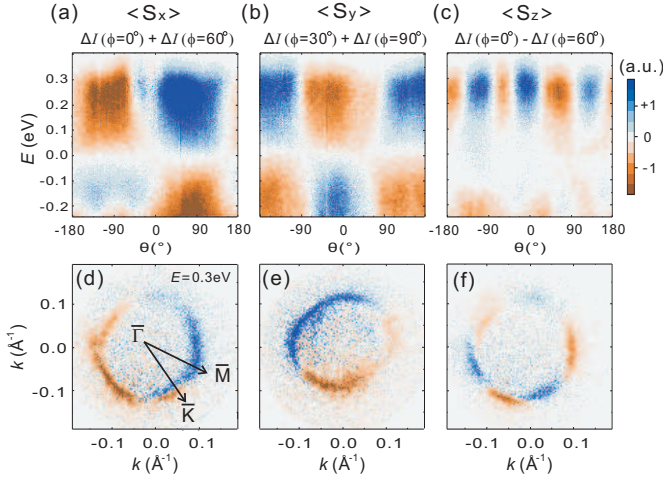


FIG. 2. (a) x , (b) y and (c) z components of the spin-texture over the complete surface states obtained by summing or subtracting ΔI data volumes at different ϕ (see text). Color maps were created by integrating the data radially in k -space over a $\pm 0.015 \text{ \AA}^{-1}$ window about the surface state contours at each energy. Constant energy cuts at the Fermi level for each spin component are shown directly below in (d) through (f).

where a and b are bandstructure dependent complex constants and Im refers to the imaginary part. Circular dichroism is obtained by taking the difference of Eq.(4) with opposite photon helicity ($A_y \rightarrow -A_y$):

$$\Delta I = a^2 \text{Im}(\mathcal{A}_x \mathcal{A}_y^*) \langle S_z \rangle_{\vec{k}} - 4ab \text{Im}(\mathcal{A}_z \mathcal{A}_y^*) \langle S_x \rangle_{\vec{k}} \quad (5)$$

Although the CD is a linear combination of $\langle S_x \rangle$ and $\langle S_z \rangle$, these can be disentangled by applying symmetry properties of $\text{Bi}_2\text{Se}_3(111)$ as follows. Time-reversal symmetry and three-fold rotational symmetry together dictate that $\langle S_z \rangle$ flips sign upon a $\Delta\phi = 60^\circ$ rotation while $\langle S_x \rangle$ stays unchanged. Taking the difference (sum) of CD patterns $\Delta\phi = 60^\circ$ apart isolates $\langle S_z \rangle$ ($\langle S_x \rangle$). The $\langle S_y \rangle$ component is trivially obtained by performing the procedure for $\langle S_x \rangle$ under a 90° sample rotation. Fig. 2 shows all three spin components measured using this method. Because calculating a and b is beyond the scope of our work, we only plot the relative and not absolute magnitude of the spins. We immediately notice that all three components reverse sign across the DP as expected and that $\langle S_x \rangle$ and $\langle S_y \rangle$ are modulated with a similar periodicity. On the other hand $\langle S_z \rangle$ exhibits a different periodicity at high energies, which vanishes in the low energy region.

To quantitatively test the validity of our microscopic theory, we first compare our extracted spin components with the ideal spin texture in the low energy region that is experimentally well-known. Constant low energy slices through the spin maps [Figs. 2(a)-(c)] show that $\langle S_z \rangle$ exhibits negligible modulation whereas $\langle S_x \rangle$ and $\langle S_y \rangle$ follow a clear $\sin(\theta)$ dependence that reverses sign across the DP [Figs. 3(a)-(c)]. By projecting the planar spin

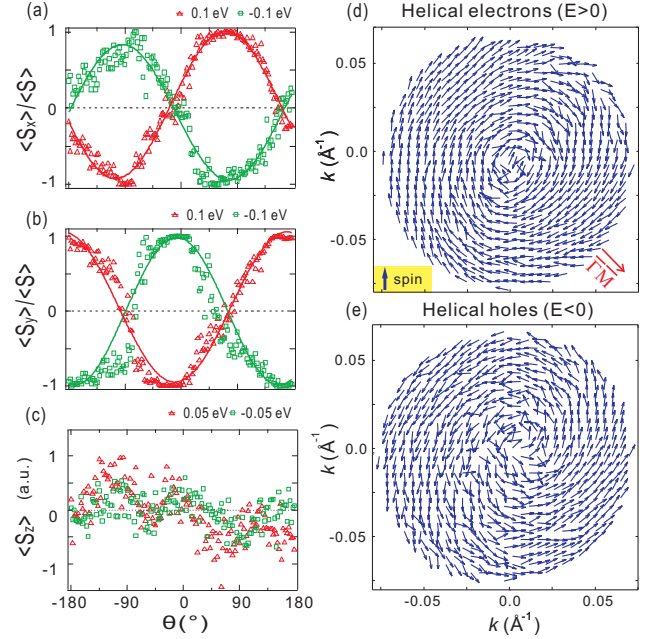


FIG. 3. The evolution of the (a) S_x , (b) S_y and (c) S_z components around constant energy contours in the vicinity of the Dirac point, obtained by taking cuts through the data in Figs. 2(b)-(d). Curves are fits to $\sin(\theta)$ and $\cos(\theta)$ varying functions for S_x and S_y respectively. (d) and (e) show the spin vectors (each normalized by its magnitude $|S|$) of all positive and negative energy states within ± 0.1 eV respectively projected onto the $k_x - k_y$ plane.

vectors of each state in the low energy region of the Dirac cone onto the $x - y$ plane, we obtain a vector field that exactly matches an ideal helical spin-texture with opposite chirality for electrons and holes [Figs. 3(d) and (e)]. We note that while the relative orientation of spins is directly measured in our experiment, the absolute sense of chirality was set by matching our data to Mott polarimetry results at a single energy-momentum point [6], although it can also be independently obtained by calculating a and b . The excellent agreement between our measured low energy CD maps and theoretical [19] and Mott polarimetry results [4–6] strongly suggests that CD-ARPES is a sensitive measure of the topological SS spin-texture.

Next we compare our CD spectra to our model in the high energy region where the spin-texture is predicted to depart from ideal planar helical form but is so far unobserved in Bi_2Se_3 using conventional Mott polarimetry based ARPES [6]. At high energies where the Fermi surface acquires a hexagonal shape, $k \cdot p$ theory predicts that the spin-texture should develop a finite out-of-plane component $\langle S_z \rangle$ that is modulated with a $\sin(3\theta)$ periodicity, with maximally upward and downward spin canting along $\bar{\Gamma}\bar{K}$ directions [19]. Fig. 4(a) shows a constant energy slice at 0.3 eV through the spin map of Fig. 2(c), where there is a clear $\sin(3\theta)$ dependence of $\langle S_z \rangle$ that is maximal along $\bar{\Gamma}\bar{K}$ and zero along $\bar{\Gamma}\bar{M}$, in per-

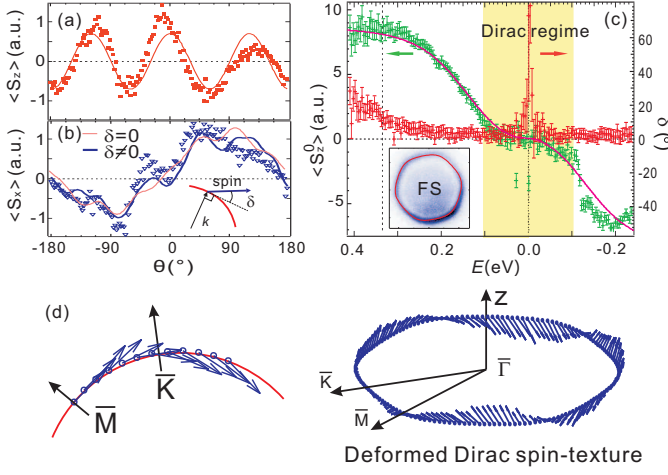


FIG. 4. Evolution of (a) S_z and (b) S_x around the Fermi surface. Red line in (a) is a fit to $k \cdot p$ theory. The blue and pink lines in (b) are fits to phenomenological models [21] that respectively do and do not account for an in-plane angular deviation (δ) away from $\vec{S} \perp \vec{k}$ locking behavior (inset). (c) The energy dependence of the amplitude of S_z modulation (green symbols), its fit (magenta line) and δ (red symbols). Inset shows the spin-integrated Fermi surface together with a fit to $k \cdot p$ theory. (d) Spin-orientation around the hexagonally deformed Fermi surface constructed from CD-ARPES data. 3D view shows spins plotted around Fermi contour and top-down view shows spins projected onto a segment of the unit circle in momentum space for ease of visualizing δ .

fect accord with both theory [19] and experiment [5] on Bi_2Te_3 . To further test whether our CD-ARPES data is indeed sensitive to spin, we compare our measured energy dependence of out-of-plane spin component along $\bar{\Gamma}\bar{K}$ ($\langle S_z \rangle^0(E)$) with its unique functional form predicted by $k \cdot p$ theory [19]:

$$\langle S_z \rangle^0(E) = 1/\sqrt{1 + [k(E)\beta]^{-4}} \quad (6)$$

where β is the only free parameter. Eq.(6) provides an excellent fit for our data [Fig. 4(c)] and the fitted value of β , which parameterizes the degree of hexagonal distortion of the Fermi surface, is quantitatively consistent with the parameters extracted from fitting the Fermi surface contour in Fig. 4(c) inset [21]. The accurate extraction of all three spin components over the entire Dirac cone from our CD-ARPES data [Fig. 4(d)] is a testament to the validity and sensitivity of our method.

While our data produce all features predicted by $k \cdot p$ theory [19], the in-plane spin component at high energies also exhibits unpredicted kinks in its θ dependence [Fig. 4(b)]. One possible origin of these kinks is that the in-plane spin magnitude is modulated purely by the out-of-plane spin canting. However a fit to the data using this assumption [Fig. 4(b) pink line] yields kinks that are too weak and fails to reproduce the nodes at $\theta = 0^\circ$ even when allowing for unrealistically large ($\sim 45^\circ$) canting angles [21]. An alternative explanation

is that the in-plane spin direction deviates from perpendicular spin-momentum locking [inset Fig. 4(b)] periodically in θ . A fit assuming periodic angular deviations of amplitude δ [Fig. 4(b) blue line] better reproduces the data. The in-plane component constructed from the data alone [Fig. 4(d)] is consistent with the latter interpretation and shows that the deviation is zero along $\bar{\Gamma}\bar{M}$ and $\bar{\Gamma}\bar{K}$ and is maximum in between the two. A plot of the amplitude of δ versus energy [Fig. 4(c)] shows that it only develops beyond $\sim 0.3\text{eV}$ from the DP. The spike exactly at the DP is consistent with spin degeneracy at the DP. This in-plane spin canting behavior has been shown by first-principles calculations as well as $k \cdot p$ expansions up to fifth order on Bi_2Te_3 [24]. However, although such effects have been observed in Rashba spin split metals [25], they have never been observed in any topological insulators.

In conclusion, we have directly observed circular dichroism from the surface states of Bi_2Se_3 . By combining a TOF-ARPES technique with ultra-pure circular photon polarization and a novel sample rotation analysis, we resolve unusual modulations in the circular dichroism photoemission pattern as a function of both energy and momentum for the first time, which closely follow the predicted three-dimensional spin-texture. A direct connection between CD-ARPES and spin-orbit induced spin-textures is established through our microscopic theory of photoemission. Our results open the possibility to generate highly-polarized spin currents with circularly polarized light, which may be detected through transport or optical means [26]. The efficiency and high spin sensitivity of our technique suggest that CD-ARPES may be used as a vectorial spin mapping tool to detect small deviations from a π Berry's phase in magnetically doped topological surface states, or to study spin-orbit coupled materials in general.

Towards completion of this manuscript, we became aware of three related concurrent and independent works [18, 27]. None, however, resolve the fine modulations in the CD-ARPES patterns that are integral to understanding the connection to spin, which is the main focus of this work.

This research is supported by Department of Energy award number DE-FG02-08ER46521, Army Research Office (ARO-DURIP) award number W911NF-09-1-0170 (ARTOF spectrometer) and in part by the MRSEC Program of the National Science Foundation under award number DMR - 0819762 (partial support for YHW). Correspondence and requests for materials should be addressed to N.G. (gedik@mit.edu).

-
- [1] J. E. Moore, Nature 464, 194 (2010)
 - [2] M. Z. Hasan, C. L. Kane, Rev. Mod. Phys. 82, 3045

- (2010)
- [3] X.-L. Qi, S.-C. Zhang, *Physics Today* 63, 33 (2010)
 - [4] D. Hsieh, et al., *Science* 323, 919 (2009); D. Hsieh, et al., *Nature* 460, 1101 (2009)
 - [5] S. Souma, et al., *Phys. Rev. Lett.* 106, 216803 (2011); S.-Y. Xu, et al., arXiv:1101.3985 (2011)
 - [6] Z.-H. Pan, et al., *Phys. Rev. Lett.* 106, 257004 (2011).
 - [7] S. Raghu, S. B. Chung, X.-L. Qi, S.-C. Zhang, *Phys. Rev. Lett.* 104, 116401 (2010).
 - [8] H.-Z. Lu, W.-Y. Shan, W. Yao, Q. Niu, S.-Q. Shen, *Phys. Rev. B* 81, 115407 (2010).
 - [9] P. Hosur, *Phys. Rev. B* 83, 035309 (2011).
 - [10] C. Westphal, J. Bansmann, M. Getzlaff, G. Schonhense, *Phys. Rev. Lett.* 63, 151 (1989);
 - [11] C. M. Schneider, J. Kirschner, *Critical Reviews in Solid State and Materials Sciences.* 20, 179 (1995);
 - [12] S. V. Halilov, et al., *J. Phys: Condens. Mat.* 5, 3851 (1993);
 - [13] F. Frentzen, et al., *Z. Phys. B* 100, 575 (1996);
 - [14] V. B. Zabolotnyy, et al., *Phys. Rev. B* 76, 024502 (2007);
 - [15] D. V. Vyalikh, et al., *Phys. Rev. Lett.* 100, 056402 (2008)
 - [16] Y. Xia, et al., *Nature Phys.* 5, 398 (2009).
 - [17] H. Zhang, et al., *Nature Phys.* 5, 438 (2009).
 - [18] Y. Ishida, et al., *Phys. Rev. Lett.* 107, 077601 (2011).
 - [19] L. Fu, *Phys. Rev. Lett.* 103, 266801 (2009).
 - [20] W. Zhang, R. Yu, H.-J. Zhang, D. Xi, Z. Fang, *New J. Phys.* 12, 065013 (2010).
 - [21] See Supplemental Material.
 - [22] S. Hufner, *Photoelectron Spectroscopy* (Springer, Berlin, 2003).
 - [23] Y.L. Chen, et al., *Science* (2009); K. Kuroda, et al., *Phys. Rev. Lett.* 105, 076802 (2010).
 - [24] S. Basak, et al., arxiv: 1103.4675 (2011)
 - [25] F. Meier, et al., *Phys. Rev. B* 77, 165431 (2008)
 - [26] D. Hsieh, et al., *Phys. Rev. Lett.* 107, 077401 (2011)
 - [27] Park et al., arXiv:1107.3285 (2011); Scholz et al., arXiv:1108.1053 (2011).